

GTPases (17). Accordingly, ADP-ribosylation of Rho GTPases by TccC5 inhibited the GTP hydrolysis catalyzed by the GTPases (Fig. 3C and fig. S8C). Thus, TccC5 may cause persistent activation of Rho GTPases by ADP-ribosylation. To confirm that the toxins caused selective modification of target proteins in intact cells, we treated HeLa cells with PTC3 or PTC5 and also with the combination of PTC3 and PTC5. As an additional control, cells were treated with TcdA1 only. Thereafter, activated RhoA and Rac proteins were identified in lysates of these cells by rhotekin and PAK pull-down assays. Furthermore, actin was ADP-ribosylated in the cell lysates by TccC3 and [<sup>32</sup>P]NAD<sup>+</sup>. Treatment of cells with PTC3 caused ADP-ribosylation of actin, which was detected by the reduction of radioactive labeling of actin by TccC3 but no activation of Rac or RhoA (Fig. 3D). PTC5 caused activation of RhoA and Rac but did not modify actin. In the presence of PTC3 and PTC5, both activation of RhoA and Rac and ADP-ribosylation of actin was determined. As expected, TcdA1 alone did not activate Rho GTPases or modify actin. Thus, PTC5 activates Rho GTPases in intact cells. Activation of RhoA is probably the reason for massive formation of stress fibers. RhoA activation by PTC5 also occurs in Sf9 insect cells (fig. S8B).

Here, we have elucidated the causal mechanisms of the alterations of the actin cytoskeleton induced by the Tc toxins and suggest a model for the mode of action of the toxins [supporting online material (SOM) text and fig.

S10]. Both TccC3 and TccC5, which enter the target cell cytosol via TcdA1, ADP-ribosylate actin and Rho-GTPases, respectively. The toxins thus cause actin clustering by means of a concerted action. TccC3 releases actin from its thymosin-β<sub>4</sub> complex, probably supplying monomeric actin to the filament-promoting activities of profilin and actin nucleators such as the formins (18, 19), and TccC5 activates signal pathways, which support stress fiber formation. In addition, because Rho GTPases are also involved in a large array of other biological functions (20, 21), their alteration by Tc toxins may be of major importance for the host-pathogen interaction of *P. luminescens*. Tc toxins are a common principle in insect pathogenicity of a broad spectrum of bacteria and have been identified in human pathogenic *Yersinia pseudotuberculosis* and *Yersinia pestis* (22, 23). Thus, the molecular mechanism of the prototypical Tc complexes aids the understanding of other types of Tc toxins in insecticidal bacteria and potentially human pathogens.

#### References and Notes

1. S. A. Joyce, R. J. Watson, D. J. Clarke, *Curr. Opin. Microbiol.* **9**, 127 (2006).
2. R. H. ffrench-Constant *et al.*, *FEMS Microbiol. Rev.* **26**, 433 (2003).
3. N. R. Waterfield, D. J. Bowen, J. D. Fetherston, R. D. Perry, R. H. ffrench-Constant, *Trends Microbiol.* **9**, 185 (2001).
4. D. Bowen *et al.*, *Science* **280**, 2129 (1998).
5. S. C. Lee *et al.*, *J. Mol. Biol.* **366**, 1558 (2007).
6. N. Waterfield, M. Hares, G. Yang, A. Dowling, R. ffrench-Constant, *Cell. Microbiol.* **7**, 373 (2005).

7. Materials and methods are available as supporting material on Science Online.
8. R. J. Fieldhouse, A. R. Merrill, *Trends Biochem. Sci.* **33**, 546 (2008).
9. H. Barth, K. Aktories, M. R. Popoff, B. G. Stiles, *Microbiol. Mol. Biol. Rev.* **68**, 373 (2004).
10. K. Aktories *et al.*, *Nature* **322**, 390 (1986).
11. K. Aktories, A. Wegner, *J. Cell Biol.* **109**, 1385 (1989).
12. E. Irobi *et al.*, *EMBO J.* **23**, 3599 (2004).
13. E. M. De La Cruz *et al.*, *Biophys. J.* **78**, 2516 (2000).
14. H. Q. Sun, K. Kwiatkowska, H. L. Yin, *Curr. Opin. Cell Biol.* **7**, 102 (1995).
15. M. Vogelsgesang, A. Pautsch, K. Aktories, *Naunyn-Schmiedeberg's Arch. Pharmacol.* **374**, 347 (2007).
16. G. Schmidt *et al.*, *Nature* **387**, 725 (1997).
17. I. R. Vetter, A. Wittinghofer, *Science* **294**, 1299 (2001).
18. M. Pring, A. Weber, M. R. Bubb, *Biochemistry* **31**, 1827 (1992).
19. S. Romero *et al.*, *Cell* **119**, 419 (2004).
20. A. B. Jaffe, A. Hall, *Annu. Rev. Cell Dev. Biol.* **21**, 247 (2005).
21. K. Burridge, K. Wennerberg, *Cell* **116**, 167 (2004).
22. J. Parkhill *et al.*, *Nature* **413**, 523 (2001).
23. M. C. Hares *et al.*, *Microbiology* **154**, 3503 (2008).
24. H. G. Mannherz *et al.*, *J. Mol. Biol.* **366**, 745 (2007).
25. We thank Agilent Technologies for supporting us with instrumentation, R. S. Goody (Dortmund, Germany) for help in stopped-flow measurements, and M. Geyer (Dortmund, Germany) for providing profilin. The study was financially supported by the Deutsche Forschungsgemeinschaft DFG to K.A. and H.G.M.

#### Supporting Online Material

www.sciencemag.org/cgi/content/full/327/5969/1139/DC1  
Materials and Methods  
SOM Text  
Figs. S1 to S10  
References

11 November 2009; accepted 22 January 2010  
10.1126/science.1184557

## Noise Can Induce Bimodality in Positive Transcriptional Feedback Loops Without Bistability

Tsz-Leung To and Narendra Maheshri\*

Transcriptional positive-feedback loops are widely associated with bistability, characterized by two stable expression states that allow cells to respond to analog signals in a digital manner. Using a synthetic system in budding yeast, we show that positive feedback involving a promoter with multiple transcription factor (TF) binding sites can induce a steady-state bimodal response without cooperative binding of the TF. Deterministic models of this system do not predict bistability. Rather, the bimodal response requires a short-lived TF and stochastic fluctuations in the TF's expression. Multiple binding sites provide these fluctuations. Because many promoters possess multiple binding sites and many TFs are unstable, positive-feedback loops in gene regulatory networks may exhibit bimodal responses, but not necessarily because of deterministic bistability, as is commonly thought.

When a cell must unambiguously commit to a particular gene expression program, often a digital change occurs in a key regulator's expression (1). Decision-making circuitry within metabolic (2), developmental (3), and synthetic gene regulatory networks

(4–6) uses positive feedback to provide bimodal, “all-or-none” expression of a regulator. The bimodal population response has been explained with deterministic models that predict bistable gene expression (7). Consider a positive-feedback loop where a transcriptional activator binds its own promoter to regulate expression. The open-loop promoter response (in the absence of feedback) is modeled by a Hill-type equation, where the Hill coefficient describes whether the response is linear (Hill coefficient = 1) or sigmoidal

(Hill coefficient > 1) before saturating. The basis for sigmoidal responses can be direct cooperative binding of transcription factors (TFs) to promoters, or indirect cooperativity via nucleosome displacement (8). Without cooperativity, bistability is not predicted.

To understand how promoter structure relates to the Hill coefficient, we used the widely used tet-Off system, adapted for budding yeast (9). The tet-transcriptional activator (tTA) binds to a tet operator (tetO) sequence in the absence of doxycycline. We constructed yeast strains without (open loop) and with feedback (closed loop), using previously designed promoters with one (1tetO) and seven (7tetO) binding sites (9). With 1tetO in positive feedback, the reporter exhibits a graded steady-state response to changes in feedback strength, whereas 7tetO exhibits a bimodal response (Fig. 1A). One explanation is that 7tetO has a sigmoidal open-loop response due to cooperative binding of tTA to multiple binding sites, resulting in bistability (6, 10). Yet, if one accounts for the binding of doxycycline to the tTA dimer [Supporting Online Material (SOM) Text], both 1tetO and 7tetO exhibit a noncooperative open-loop response, with a Hill coefficient of ~1 (Fig. 1B). To eliminate the possibility of altered doxycycline binding, we titrated tTA levels directly, using a galactose-inducible promoter, and confirmed the

Department of Chemical Engineering, Massachusetts Institute of Technology, Cambridge, MA 02139, USA.

\*To whom correspondence should be addressed. E-mail: narendra@mit.edu

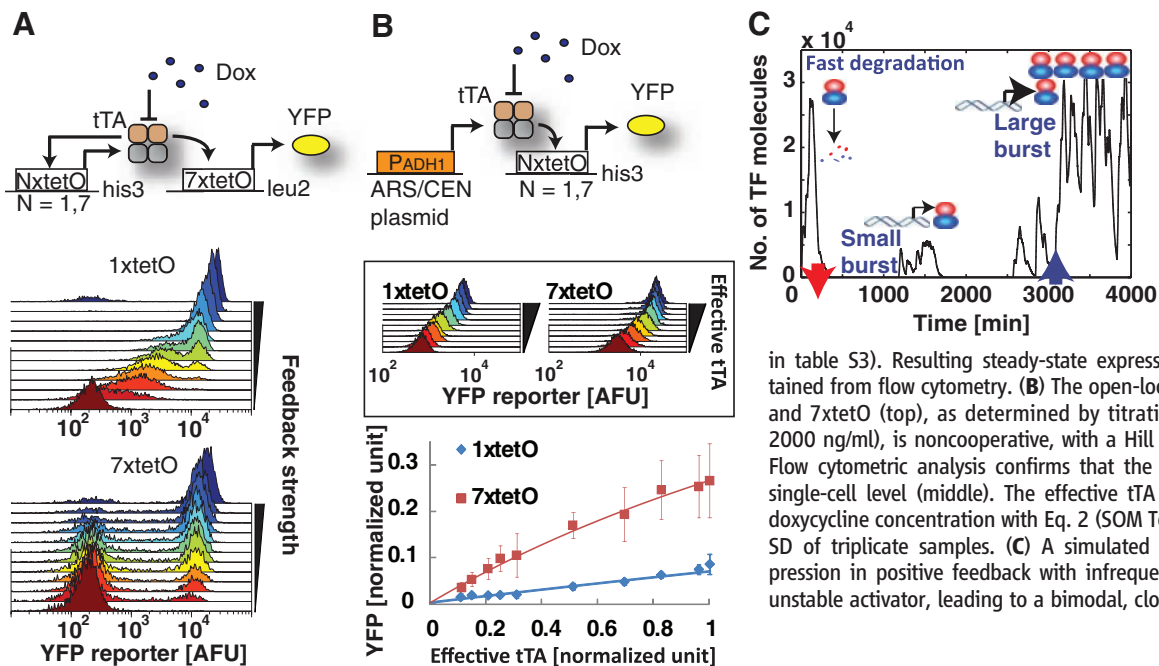


**Fig. 1.** Bimodal gene expression with noncooperative positive feedback. **(A)** Yeast strains engineered with 1xtetO and 7xtetO in a closed-loop configuration (top) were grown to steady state. Feedback strength was modulated by varying doxycycline concentration from 0 to 2000 ng/ml (bottom) (details in table S3). Resulting steady-state expression distributions were obtained from flow cytometry. **(B)** The open-loop response of both 1xtetO and 7xtetO (top), as determined by titration with doxycycline (0 to 2000 ng/ml), is noncooperative, with a Hill coefficient of ~1 (bottom). Flow cytometric analysis confirms that the response is graded at the single-cell level (middle). The effective tTA level was calculated from doxycycline concentration with Eq. 2 (SOM Text). Error bars indicate the SD of triplicate samples. **(C)** A simulated time series describing expression in positive feedback with infrequent promoter firing and an unstable activator, leading to a bimodal, closed-loop response.

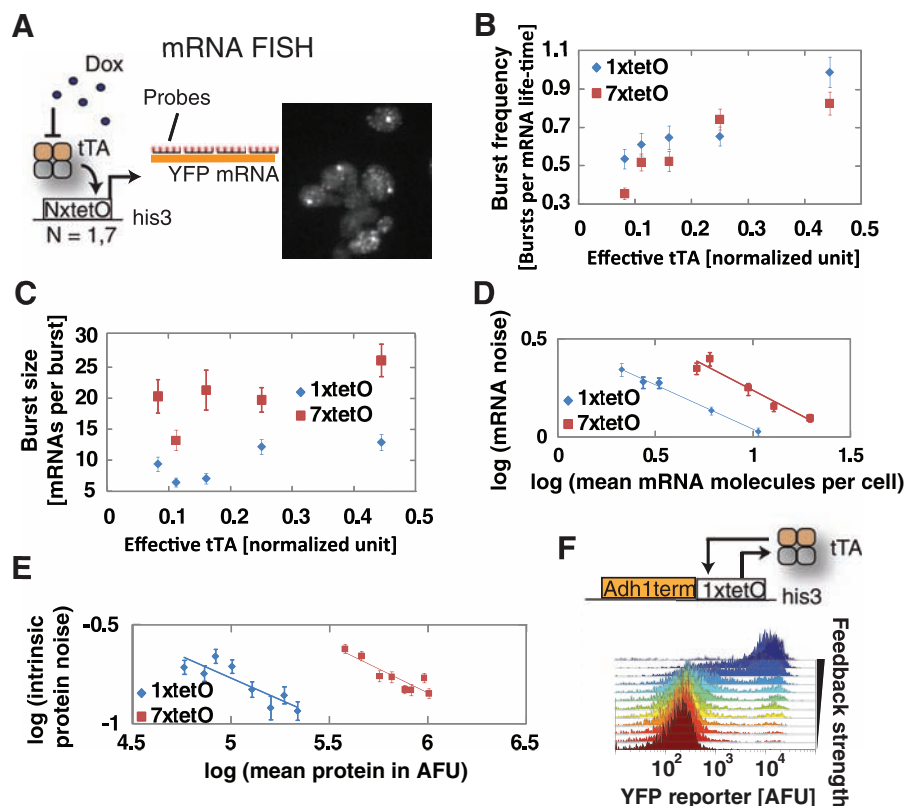


**Fig. 2.** Multiple TF binding sites increase promoter noise. **(A)** The burst statistics of mRNA of 1xtetO and 7xtetO promoters were determined by mRNA FISH (24). The effective tTA level was modulated with doxycycline (250, 500, 750, 1000, and 1250 ng/ml). **(B)** The burst frequency and **(C)** burst size were inferred by fitting the steady-state mRNA distributions to a stochastic model (SOM). Error bars represent 95% confidence intervals (CIs). **(D)** The scaling law (slope ~ -0.5 on the log-log plot) between mRNA noise and mean mRNA expression level suggests that mRNA noise is primarily due to intrinsic sources and burst frequency regulation. **(E)** The intrinsic protein noise was determined by the dual-reporter assay (16). The same scaling law applies to the intrinsic protein noise. Error bars in **(D)** and **(E)** representing 95% CIs were obtained by bootstrapping. **(F)** The Adh1term-1xtetO promoter was created by inserting an ADH1 terminator upstream of 1xtetO in the sense direction. The feedback strength was modulated by varying doxycycline from 0 to 1000 ng/ml (details in table S3).

noncooperative response (fig. S1). In addition, the open-loop response of both promoters in a strain that contains a closed-loop promoter is also noncooperative (fig. S2).

Recent single-molecule approaches have revealed that gene expression often occurs in random bursts of transcription and/or translation [reviewed in (11)]. Burst statistics can be characterized by the burst size (number of mRNAs or proteins produced per transcriptional activation event) and the burst frequency (number of transcriptional activation events per mRNA or protein lifetime). A theoretical study of the effects of these stochastic bursts by Friedman *et al.* (12) predicts that bimodal expression at steady state is possible with positive feedback even when the open-loop response is noncooperative with a Hill coefficient  $\leq 1$  [similar results reported in (13)]. This requires that the maximum burst frequency is low, the burst size is large enough to turn the promoter on in positive feedback, and the activator regulates burst frequency (exact conditions shown in fig. S6). Infrequent transcriptional bursts of mRNA lead to bursts of a transcriptional activator. Simulations under these conditions (Fig. 1C) show that some bursts lead to large activator levels because of large burst sizes and switch the system to high expression (~3000 min). Because the activator is short-lived, occasionally all activators degrade before the next burst occurs (time ~300 min). This switches the system back to low expression.

We hypothesized that the 7xtetO promoter had a lower maximum burst frequency and larger burst size versus the 1xtetO promoter. Independent support for this hypothesis comes from a study of stochastic gene expression using the tet-Off system in mammalian cells (14). As in that study, we combined mRNA fluorescence in situ

hybridization (FISH) measurements (15) with a stochastic model of gene expression to determine the burst statistics of mRNA (Fig. 2A). The 7xtetO promoter has a burst size twice as high as that of the 1xtetO promoter (Fig. 2C), whereas the mRNA distributions are consistent with burst frequency regulation (Fig. 2B and fig. S7). Both mRNA and intrinsic protein noise scale with the inverse square root of abundance (Fig. 2, D and E), suggesting that mRNA noise is dominated by intrinsic fluctuations (16, 17) and tTA regulates burst frequency (18).

In the open-loop context, the *ADHI* promoter-driven tTA level was not high enough to saturate either promoter. Therefore, we used the closed-loop data, where tTA levels are much higher, to

estimate the maximum burst frequency (fig. S2). Consistent with our hypothesis and the mammalian study (14), 7xtetO has a maximum burst frequency one-fifth that of 1xtetO. Taken together, multiple tetO binding sites make a promoter more sensitive to tTA, with a lower burst frequency and a higher burst size. We were unable to determine if the increased burst size is due to a longer-duration burst or a more intense burst (fig. S9). A 1xtetO promoter variant containing the yeast *ADHI* terminator upstream of the 1xtetO site has a non-cooperative open-loop response (fig. S11) and also exhibits a bimodal response in positive feedback (Fig. 2F). This promoter has a higher burst size and lower maximum burst frequency compared to 1xtetO (fig. S12 and table S8). Therefore, as

expected by the theory, the noise properties of the promoter, and not multiple binding sites per se, are responsible for the bimodal response.

A strong prediction of our model is that stabilization of tTA will increase the maximum burst frequency and eliminate bimodal expression. Global measurements of protein stability in yeast reveal that TFs tend to be less stable than typical proteins (19). Although tTA (a fusion between tet repressor and the VP16 activation domain) stability has not been determined, the in vivo half-life of a *lexA*-VP16 fusion protein in yeast was 6 min (20). Moreover, mono-ubiquitination of *lexA*-VP16 was required to activate the TF, but led to subsequent polyubiquitination via Met30p, targeting it for degradation (20). To stabilize tTA, we expressed the active monoubiquitinated version and deleted *MET30* (21). As expected, the closed-loop response of the stabilized tTA was more graded (Fig. 3A).

To verify whether a stochastic model could quantitatively describe our results, we measured tTA mRNA and protein half-lives. To determine the mRNA stability, we stopped transcription in a 7xtetO closed-loop strain by adding doxycycline and the transcriptional inhibitor thiolutin. Cells were fixed at specific time points after inhibition, and tTA and YFP (yellow fluorescent protein) mRNA abundance was measured by FISH. Both transcripts have a half-life of ~15 to 20 min (fig. S14). We determined the tTA stability at the population level by stopping tTA production and following tTA levels by Western blotting (Fig. 3B). tTA appears to have an ~70-min half-life, much longer than the 6-min half-life of *lexA*-VP16 (20). With the resulting high maximum burst frequency, neither the Friedman model nor a modified version accounting for all three stages (promoter, mRNA, and protein) of gene expression (SOM Text) even qualitatively describes bimodal expression. Given the short half-life of the *lexA*-VP16 fusion, we suspected that multiple forms of tTA were present in the cell and only the active form was unstable. Because activation-coupled degradation of tTA occurs only in the nucleus, we hypothesized that cytoplasmic tTA was stable and nuclear transport of tTA was slow. Nuclear transport of the reverse tTA is limiting in yeast, and addition of nuclear localization signals (NLS) alters its subcellular distribution (22).

To test the effect of nuclear transport, we fused a mammalian NLS to tTA, confirmed the nuclear localization (fig. S17), and measured the open- and closed-loop responses. As before, the NLS-tTA open-loop response was graded (fig. S15). The closed-loop responses remained bimodal for 7xtetO (Fig. 4A), although more cells were found with intermediate expression levels compared to tTA (Fig. 1A). NLS-tTA stability was reduced to a ~10-min half-life (Fig. 3B), suggesting that the increased stability of tTA was indeed due to a stable cytoplasmic fraction not susceptible to rapid degradation. By incorporating both nuclear transport and the shorter tTA half-life in our model (fig. S16), we could recapitulate the closed-loop responses for

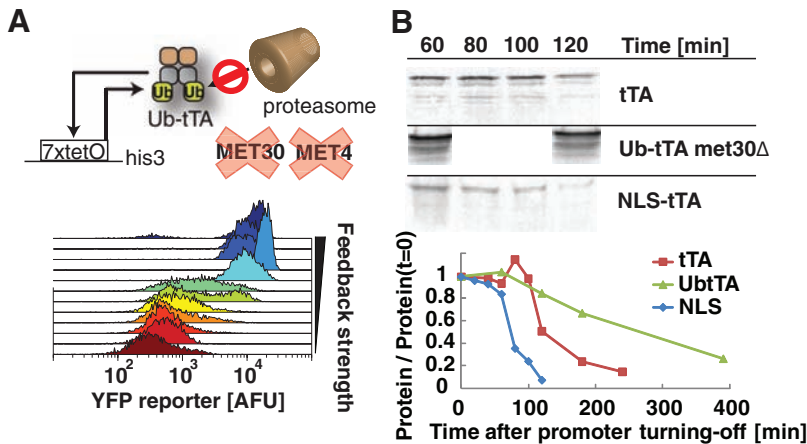
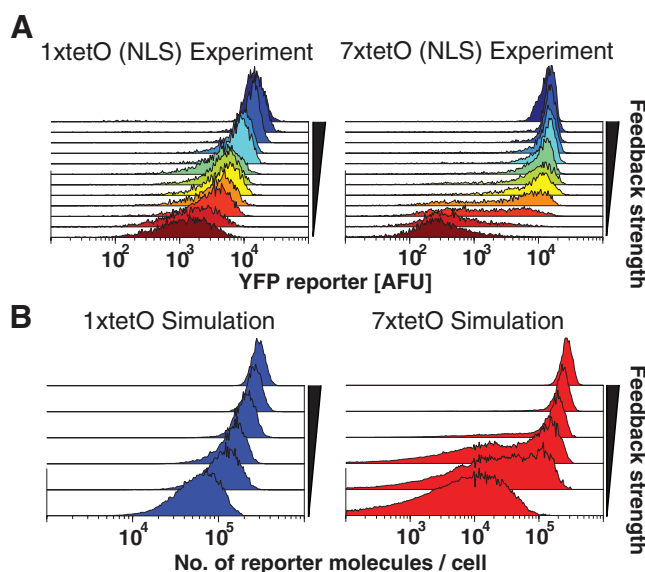


**Fig. 3.** Stabilizing the TF reduces stochastic fluctuation and eliminates bimodality. (A) To create a stabilized TF, a ubiquitin-tTA fusion was expressed in a *met30Δ met4Δ* background (upper panel) (20). The closed-loop reporter response measured by flow cytometry becomes more graded for 7xtetO (lower panel). Feedback strength was modulated by varying doxycycline, as in Fig. 1A. (B) To determine tTA stability, its expression was halted via a galactose-inducible promoter (27), and levels were measured by quantitative Western blotting. Lanes contain equivalent amount of total protein as determined by Bradford assay. After accounting for the 60-min lag required for mRNA depletion and tTA folding, tTA was found to have an ~70-min half-life. The stabilized tTA variant has an ~175-min half-life, similar to the doubling time. The SV40 NLS-tagged tTA has an ~15-min half life, suggesting that nuclear transport was rate limiting.

**Fig. 4.** Stochastic modeling of the closed-loop response reveals the importance of nuclear transport. (A) A SV40 NLS was fused to the N terminal of tTA, and the closed-loop reporter response at steady state was measured by flow cytometry. The feedback strength was modulated by varying doxycycline concentration, as in Fig. 1A. The measured expression profiles for NLS-tTA remain bimodal, but less so compared to normal tTA (Fig. 1A). (B) Stochastic simulations using the scheme in fig. S16 and parameter values in tables S3 and S7. Results capture differences between the graded versus bimodal expression profiles between 1xtetO and 7xtetO and generally agree with experimental closed-loop NLS-tTA data.



NLS-tTA (Fig. 4B) using measured in vivo parameters for the open-loop promoters (table S7) (23).

This work is related to examples where enzymatic cycles (24) and positive feedback in spatial organization (25) possess bimodal activity that is solely due to stochastic fluctuations. In addition, a stochastic view of noncooperative positive feedback in HIV escape from latency leads to a transient bimodal response (26), but we demonstrated a steady-state bimodal response. The hallmarks of noise-induced bimodality in gene expression—positive-feedback loops and unstable proteins—are characteristic of many TFs and promoters and likely widespread in biological systems (table S4). Our findings also suggest that multiple binding sites may be associated with all-or-none responses not by virtue of cooperative binding but because of increased noise. Finally, this work provides new guidelines for the construction of a bistable switch based on positive feedback for applications in synthetic biology and metabolic engineering.

#### References and Notes

- U. Alon, *An Introduction to Systems Biology: Design Principles of Biological Circuits* (CRC Press, Boca Raton, FL, 2006).
- M. Acar, A. Becskei, A. van Oudenaarden, *Nature* **435**, 228 (2005).
- W. Xiong, J. E. Ferrell Jr., *Nature* **426**, 460 (2003).
- N. T. Ingolia, A. W. Murray, *Curr. Biol.* **17**, 668 (2007).
- F. J. Isaacs, J. Hasty, C. R. Cantor, J. J. Collins, *Proc. Natl. Acad. Sci. U.S.A.* **100**, 7714 (2003).
- C. M. Ajo-Franklin *et al.*, *Genes Dev.* **21**, 2271 (2007).
- A. D. Keller, *J. Theor. Biol.* **172**, 169 (1995).
- J. A. Miller, J. Widom, *Mol. Cell. Biol.* **23**, 1623 (2003).
- E. Garí, L. Piedrafita, M. Aldea, E. Herrero, *Yeast* **13**, 837 (1997).
- A. Becskei, B. S raphin, L. Serrano, *EMBO J.* **20**, 2528 (2001).
- N. Maheshri, E. K. O'Shea, *Annu. Rev. Biophys. Biomol. Struct.* **36**, 413 (2007).
- N. Friedman, L. Cai, X. S. Xie, *Phys. Rev. Lett.* **97**, 168302 (2006).
- R. Karmakar, I. Bose, *Phys. Biol.* **4**, 29 (2007).
- A. Raj, C. S. Peskin, D. Tranchina, D. Y. Vargas, S. Tyagi, *PLoS Biol.* **4**, e309 (2006).
- A. Raj, P. van den Bogaard, S. A. Rifkin, A. van Oudenaarden, S. Tyagi, *Nat. Methods* **5**, 877 (2008).
- M. B. Elowitz, A. J. Levine, E. D. Siggia, P. S. Swain, *Science* **297**, 1183 (2002).
- A. Bar-Even *et al.*, *Nat. Genet.* **38**, 636 (2006).
- There is sizable extrinsic noise in protein abundance as measured by fluorescence (fig. S10), yet it does not appear to have a major effect (SOM Text).
- A. Belle, A. Tanay, L. Bitincka, R. Shamir, E. K. O'Shea, *Proc. Natl. Acad. Sci. U.S.A.* **103**, 13004 (2006).
- S. E. Salghetti, A. A. Caudy, J. G. Chenoweth, W. P. Tansey, *Science* **293**, 1651 (2001).
- MET4* must also be deleted, as single deletion of *MET30* is lethal (20).
- A. Becskei, M. G. Boselli, A. van Oudenaarden, *Nat. Cell Biol.* **6**, 451 (2004).
- The more pronounced bimodal response from nuclear transport-limited tTA (Fig. 1A) compared to NLS-tTA remains unclear, but likely depends on details of tTA transport (see SOM).
- M. Samoilov, S. Plyasunov, A. P. Arkin, *Proc. Natl. Acad. Sci. U.S.A.* **102**, 2310 (2005).
- S. J. Altschuler, S. B. Angenent, Y. Wang, L. F. Wu, *Nature* **454**, 886 (2008).
- L. S. Weinberger, T. Shenk, *PLoS Biol.* **5**, e9 (2007).
- Materials and methods are available as supporting material in *Science* Online.
- We thank A. Raj for technical assistance with FISH, and C. J. Zopf, H. Kim, A. Raj, J. Gore, and K. Verstrepen for comments on the manuscript. This work was funded by an NSF Graduate Fellowship (to T.-L. T.), the Human Frontiers Science Program RGY2007 (to N.M.), and Massachusetts Institute of Technology startup funds (to N.M.).

#### Supporting Online Material

www.sciencemag.org/cgi/content/full/327/5969/1142/DC1  
Material and Methods  
SOM Text  
Figs. S1 to S19  
Tables S1 to S9  
References

10 July 2009; accepted 8 January 2010  
10.1126/science.1178962

## Cortical Plasticity Induced by Inhibitory Neuron Transplantation

Derek G. Southwell,<sup>1</sup> Robert C. Froemke,<sup>2</sup> Arturo Alvarez-Buylla,<sup>1,\*</sup> Michael P. Stryker,<sup>3,\*</sup> Sunil P. Gandhi<sup>3,\*</sup>

Critical periods are times of pronounced brain plasticity. During a critical period in the postnatal development of the visual cortex, the occlusion of one eye triggers a rapid reorganization of neuronal responses, a process known as ocular dominance plasticity. We have shown that the transplantation of inhibitory neurons induces ocular dominance plasticity after the critical period. Transplanted inhibitory neurons receive excitatory synapses, make inhibitory synapses onto host cortical neurons, and promote plasticity when they reach a cellular age equivalent to that of endogenous inhibitory neurons during the normal critical period. These findings suggest that ocular dominance plasticity is regulated by the execution of a maturational program intrinsic to inhibitory neurons. By inducing plasticity, inhibitory neuron transplantation may facilitate brain repair.

Once in life, a critical period for ocular dominance plasticity is initiated by the development of intracortical inhibitory synaptic transmission (1). Reduction of inhibitory transmission disrupts ocular dominance plasticity (2), whereas the early enhancement of inhibitory transmission promotes a precocious

period of ocular dominance plasticity (3–6). After the critical period has passed, however, direct pharmacological augmentation of inhibitory transmission does not induce plasticity (7).

Cortical inhibitory neurons are produced in the medial and caudal ganglionic eminences of the embryonic ventral forebrain (8–10). When transplanted into the brains of older animals, embryonic inhibitory neuron precursors disperse widely (11) and develop the characteristics of mature cortical inhibitory neurons (12). We have used repeated optical imaging of intrinsic signals (13, 14) to examine whether inhibitory neuron transplantation produces ocular dominance plasticity after the critical period (fig. S1).

In mice, ocular dominance plasticity reaches a peak in the fourth postnatal week, when cortical inhibitory neurons are ~33 to 35 days old

(3, 10) (Fig. 1A). At this age, monocular visual deprivation shifts neuronal responses in the binocular visual cortex away from the deprived eye and toward the nondeprived eye. Throughout this study, we have quantified the balance of cortical responses to the two eyes by calculating an ocular dominance index (ODI). An ODI value of –1 indicates responses dominated by the ipsilateral eye, a value of 1 represents responses dominated by the contralateral eye, and a value of 0 represents equal binocular responses. In untreated mice at the peak of the critical period [postnatal day 28 (P28)], the binocular visual cortex responded more to the contralateral eye, with a mean ODI of 0.22 (Fig. 1B, open black circles). After four days of visual deprivation of the contralateral eye, cortical responses were shifted toward the ipsilateral eye, with a mean ODI value of 0.00 (Fig. 1B, filled black circles).

We first examined whether inhibitory neuron transplantation induced ocular dominance plasticity 14 to 18 days after the critical period, at P42 to 46. We transplanted cells from the embryonic day 13.5 to 14.5 (E13.5 to 14.5) medial ganglionic eminence (MGE) into sites flanking the host primary visual cortex at two ages, P0 to 2 and P9 to 11, respectively (Fig. 1A). Host mice that received transplants at P9 to 11 were thus studied 33 to 35 days after transplantation (DAT), whereas hosts that received transplants at P0 to 2 were studied 43 to 46 DAT. Transplantation did not alter the absolute magnitudes of visual responses in the host binocular visual cortex (fig. S2). Before monocular deprivation, host cortex responded more to the contralateral eye (Fig. 1B; P9 to 11 hosts, 33 to 35 DAT ODI mean  $\pm$  SD = 0.23  $\pm$  0.02, open green squares; P0 to 2 hosts, 43

<sup>1</sup>Department of Neurological Surgery and the Eli and Edythe Broad Center of Regenerative Medicine and Stem Cell Research, University of California, San Francisco, 513 Parnassus Avenue, San Francisco, CA 94143, USA. <sup>2</sup>Department of Otolaryngology, University of California, San Francisco, 513 Parnassus Avenue, San Francisco, CA 94143, USA. <sup>3</sup>Department of Physiology, University of California, San Francisco, 513 Parnassus Avenue, San Francisco, CA 94143, USA.

\*To whom correspondence should be addressed. E-mail: abuylla@stemcell.ucsf.edu (A.A.B.); stryker@phy.ucsf.edu (M.P.S.); sunil@phy.ucsf.edu (S.P.G.)